ORIGINAL RESEARCH

Targeted Nanobubbles of PD-L1 mAb Combined with Doxorubicin as a Synergistic Tumor Repressor in Hepatocarcinoma

Yezi Chen [iD][1,2,]*, Xiaoqin Luo[2,3,]*, Yun Liu[4], Yunlei Zou[1,2], Shiqi Yang [iD][1,2], Chaoqi Liu[1,2], Yun Zhao [iD][1,2]

[1]Hubei Key Laboratory of Tumor Microenvironment and Immunotherapy, China Three Gorges University, Yichang, People's Republic of China; [2]Medical College of China Three Gorges University, Yichang, People's Republic of China; [3]Department of Medical Imaging Center, Renmin Hospital Affiliated to Hubei University of Medicine, Shiyan, People's Republic of China; [4]Department of Ultrasonography, Yichang Central People's Hospital, Yichang, People's Republic of China

*These authors contributed equally to this work

Correspondence: Yun Zhao; Chaoqi Liu, Medical College of China Three Gorges, University, Yichang, People's Republic of China, Email zhaoyun@ctgu.edu.cn; ctgulcq@163.com

Purpose: Ultrasound nanobubbles (NBs) can kill tumor cells, mediated by their effects of cavitation and acoustic perforation through ultrasound, while as novel drug carriers, biomaterial-modified NBs release drugs at a target region. In this work, the ultrasound NBs bridged by biotin-streptavidin were prepared simultaneously to be loaded with both programmed death ligand 1 monoclonal antibody (PD-L1 mAb) and doxorubicin (DOX), which are immune checkpoint inhibitors (ICIs) and chemotherapeutic agents, to synergize immunotherapy and chemotherapy combined with sonodynamic therapy (SDT).

Methods: The PD-L1 mAb/DOX NBs, using bridging affinity biotin (BRAB) technology as a bridge, were prepared by thin-film hydration and mechanical oscillation for the targeted delivery of biotinylated PD-L1 mAb and DOX. Characterization and pharmacokinetic studies of PD-L1 mAb/DOX NBs were performed in vitro and in vivo. The antitumor effect of ultrasound-mediated PD-L1 mAb/DOX-NBs was studied in the subcutaneously transplanted tumor of the H22 hepatoma model, and the mechanism of synergistic tumor repression was investigated.

Results: The data of in vitro targeting experiments, contrast-enhanced ultrasound imaging (CEUS), in vivo imaging of the small animals imaging system (IVIS), and frozen sections showed that PD-L1 mAb/DOX-NBs have well-targeted aggregation in the tumor. By observing tumor inhibition rate, tissue cell apoptosis, and apoptosis-related gene and protein expression, the PD-L1 mAb/DOX-NBs group showed the best immunotherapy effects, and its tumor volume and mass inhibition rates were about 69.64% and 75.97%, respectively ($P < 0.01$). Therefore, blocking the PD-1/PD-L1 pathway could improve immune cells' tumor-killing ability. Antitumor immune cytokines were further enhanced when combined with DOX-induced tumor cell apoptosis and immunogenic cell death (ICD).

Conclusion: In summary, ultrasound-mediated PD-L1 mAb/DOX-NBs showed significant synergistic antitumor effects, providing a potential combined immunotherapy strategy for HCC.

Keywords: ultrasound targeted nanobubble destruction, tumor immune therapy, immune checkpoint inhibitors, immunogenic cell death, drug delivery

Introduction

Hepatocellular carcinoma (HCC) is one of the most common malignant tumors of the digestive system, accounting for over 90% of all primary liver cancers. The global incidence of HCC ranks fifth in malignant tumors, and its mortality rate ranks third.[1] The main treatments for HCC are surgical resection, liver transplantation, and local ablation. However, most patients with HCC are already at an advanced stage or have metastases at the time of diagnosis and have lost the opportunity for radical treatment. Therefore, exploring new HCC treatment methods is of great significance.

Cancer immunotherapy is an emerging and rapidly developing strategy for malignant tumors. It mainly reactivates and strengthens the immune system to recognize and attack cancer cells specifically and produces immune memory to permanently inhibit tumor development.[2–4] In the tumor microenvironment, highly expressed programmed death-ligand 1 (PD-L1) on the surface of tumor cells specifically binds to PD-1 on the surface of activated T cells to inhibit the activation and proliferation of T cells, leading to the depletion and apoptosis of tumor-specific T cells, thus enabling tumor cells to escape immune surveillance.[5,6] Therefore, blocking the PD-1/PD-L1 pathway can prevent immune system tolerance and enhance T-cell effector function to kill cancer cells. Studies have shown that PD-L1 is overexpressed in liver cancer cells and is significantly associated with tumor invasiveness, overall survival, and postoperative recurrence, suggesting that PD-L1 can be used as a therapeutic target and potential biomarker for liver cancer.[7,8] In recent years, PD-1/PD-L1 immune checkpoint inhibitor (ICI) therapy has shown great promise in the treatment of various cancers, such as advanced renal cancer,[9] liver cancer,[10] urothelial cancer,[11] and non-small cell lung cancer.[12] It has resulted in higher response rates, remission rates, and better overall survival, significantly improving the prognosis of cancer patients.

Doxorubicin (DOX), as an anthracycline chemotherapeutic drug, can inhibit DNA topoisomerase II, cause DNA damage, and induce cell apoptosis. At the same time, DOX can also induce immunogenic cell death (ICD), resulting in the release or exposure of damage-related molecular patterns (DAMPs), including surface exposure of calreticulin (CRT), high mobility group box B1 (HMGB1), and adenosine triphosphate release (ATP), which amplify the antigen-presenting ability of dendritic cells (DCs) and activate tumor-specific CTLs to recognize and attack tumor cells.[13,14]

Sonodynamic therapy (SDT) is a non-invasive anticancer therapy, in which ultrasound penetrates biological tissues with low intensity and activates sonosensitive agents enriched in tumor sites, resulting in tumor cell damage or even death. Furthermore, tumor-related antigens can be released to trigger ICD,[15,16] thus promoting DC maturation and enhancing the antitumor immune response. As a sonosensitizer, DOX can promote the oxidative damage of mitochondria under low-intensity ultrasound excitation, thereby inducing apoptosis.[17] However, due to its poor water solubility and targeting, short blood retention time, and uncontrollable pharmacokinetics, the clinical application of DOX shows great limitations.[18] The application of effective antitumor doses will inevitably produce high toxicity to normal cells, causing a series of toxic side effects, and low-dose drug stimulation can gradually lead to drug resistance. At present, many efforts have been made to improve the efficacy of DOX drug delivery to reduce its toxic side effects and drug resistance. Therefore, a well-designed carrier delivering an effective dose of DOX to the tumor site displays great clinical significance. Diverse biomaterials have been investigated as vehicles for DOX delivery. For example, peptide-based delivery systems have been used to deliver small molecule anticancer drugs such as DOX.[19] Nanobowl-supported liposomal DOX enhances the stability of actively loaded liposomal DOX by embedding a rigid nanobowl in the liposome water cavity.[20] DOX is easily adsorbed onto the surface of carbon nanotubes through π-π stacking, making a carbon nanotube-DOX conjugation as the basis for the carbon nanotube-based drug delivery system for DOX delivery to cancer cells.[21] In this work, we designed and synthesized nanobubbles (NBs) for the co-delivery of PD-L1 mAb and DOX to target DOX delivery and achieve a synergistically enhanced antitumor effect.

NBs, as new drug delivery carriers, carry drugs that can be passively released in the target tissue upon their in vitro ultrasound irradiation at a fixed point. Targeted NBs couple peptides, antibodies, or other ligands with targeting specificity on the their membrane and selectively bind to highly expressed antigens or receptors at the lesion site, thereby delivering targeted drugs to the lesion site.[22,23] An NB is usually composed of an outer shell and an encapsulated gas core, with a spherical shape and a diameter of nanometers. However, the advantage of targeted NBs prepared in this work is that they have a small enough particle size to penetrate the blood vessel wall and enter the tumor tissue. Due to the incomplete tumor vascular basement membrane, enlarged vascular endothelial cell space (about 380–780 nm), and lack of lymphatic drainage, NBs can preferentially accumulate passively at tumor sites, which is called the enhanced permeability and retention (EPR) effect.[24] The PD-L1 mAb attached to the surface of NBs can selectively bind to PD-L1, a specific marker of tumor vasculature, thereby enhancing targeting efficiency and promoting the accumulation of intratumoral NBs. Meanwhile, NBs can be burst by combined in vitro ultrasound fixed-point irradiation to achieve the controlled release of the drug in the target area, as a targeted therapy.

Thus, in this study, the method of ultrasound-triggered NBs drug delivery targeting was implemented to improve local drug concentrations and limit drug uptake by normal cells, thus significantly enhancing therapeutic effects and reducing

systemic toxicity and side effects,[25,26] and to evaluate synergistic antitumor mechanisms in the immune responses of ultrasound-mediated PD-L1 mAb/DOX-NBs on HCC xenografts.

Materials and Methods
Cell Lines and Animals
Mouse hepatocarcinoma cell lines Hepa1-6 and H22 were purchased from the China Center for Type Culture Collection (CCTCC, Wuhan, China) and stored at the Three Gorges University Tumor Microenvironment and Immune Therapy Laboratory. The Hepa1-6 cell line was cultured in DMEM (Thermo Fisher, Waltham, MA, USA), and the H22 cell line was cultured in 1640 (Thermo Fisher, Waltham, MA, USA), both supplemented with 10% fetal bovine serum (FBS, Thermo Fisher) and 1% penicillin/streptomycin (Solarbio life sciences, Beijing, China) at 37°C under 5% CO_2.

Female BALB/c normal mice (6–8 weeks, 18–20 g) were purchased from the Wuhan Institute of Biological Products Co., Ltd. (Wuhan, China). All mice were kept under specific pathogen-free conditions in the Animal Experimental Center of China Three Gorges University (Hubei, China). All animal experiments were approved by the Animal Experimental Committee of China Three Gorges University (Hubei, China)(ethical approval numbers:2021030CB). All procedures were performed following the guidelines of the Ministry of Science and Technology of the People's Republic of China.

Preparation of PD-L1 mAb/DOX-NBs
Based on the strong affinity between biotin and streptavidin, PD-L1 mAb/DOX-NBs in this experiment were prepared using membrane hydration and the mechanical oscillation method. We mixed 1,2-dipalmitoyl-sn-glycero-3-phosphocholine (DPPC, Avanti Polar Lipids, INC, USA),1,2-distearoyl-sn-glycero-3-phosphoethanolamine-N-[methoxy (polyethylene glycol)-2000] (DSPE-PEG2000, Avanti Polar Lipids, INC, USA), 1.2-distearoyl-sn-glycero-3-phosphoethanolamine-N-[biotinyl (polyethylene glycol)-2000] (DSPE-PEG2000-Biotin, Avanti Polar Lipids, INC, USA),3β-[N-(N', N'-dimethylaminoethane) carbamoyl] cholesterol (DC-Chol, Avanti Polar Lipids, Inc, USA) and DOX (Cayman Chemical, USA) in a clean flask with a mass ratio of 5:1:1:0.5:0.35, and a sufficient amount of chloroform was added to fully dissolve them. After removing the chloroform with a rotary evaporator (Precision HLG3; Heidolph), a uniform phospholipid film appeared on the bottle wall. Then, a mixture of PBS and glycerin with a volume ratio of 9:1 was added to the bottle and placed in a water bath to completely dissolve the film. The mixture was divided into vials, evacuated, and filled with C3F8 gas (Wuhan Niuride Special Gas Co., Ltd., Wuhan, China). Finally, it was shaken at high speed for 90 seconds in a silver-mercury mixer (SI Vortex-Genie 2; Scientific Industries; Thermo Fisher Scientific, Inc.) to obtain biotinylated DOX NBs. After standing, 100 μL of biotinylated DOX NBs were taken, and sufficient streptavidin was added and incubated for 1 h on a 4°C shaker. Then, 6 μg of biotinylated PD-L1 antibody (eBioscience, San Diego, Calif, USA) were added to the NBs and incubated for 1 hour on a 4°C shaker to obtain PD-L1 mAb/DOX-NBs. NBs were stored at 4°C after sterilization.

Morphological Characterization and Particle Size
After diluting the prepared PD-L1 mAb/DOX-NBs, their morphology and distribution were observed under a fluorescence microscope and a scanning electron microscope (SEM; JSM-7500F, JEOL, Tokyo, Japan). The average particle size of PD-L1 mAb/DOX-NBs was detected by Zetasizer Nano ZS (Malvern Panalytical).

The Encapsulation Rate of DOX or PD-L1 mAb in the Nanobubbles
The DOX encapsulation rate was detected by the thin-film dialysis method. The UV-Vis absorption spectrum of DOX was determined by UV spectrophotometry. The maximum absorption and standard curve of DOX were then obtained by this method. The DOX-NBs were dialyzed using dialysis bags (Union Carbide, US) for 6 hours to filter the free DOX and then mixed with methyl alcohol to dissolve the NBs. The mixture was now the DOX all loaded into the NBs. Next, the OD of the mixture was measured at the maximum absorption, and the amount of DOX was calculated according to the standard curve. Finally, the encapsulation rate was calculated using the following formula: Encapsulation rate (%) = (amount of DOX loaded into NBs/total amount of DOX material) x 100%.

To visualize the binding between biotinylated DOX NBs and PD-L1 antibody, the prepared PD-L1mAb/DOX-NBs were co-incubated with FITC-labeled biotinylated PD-L1 antibody for 1 hour. The binding between NBs and the antibody was observed under confocal laser scanning microscopy (CLSM; Nikon Corporation, Tokyo, Japan), and the binding rate was further detected by flow cytometry.

ROS Assay

To investigate the cellular reactive oxygen species (ROS) stress stimulated by the ultrasound and the NBs, Hepa1-6 cells were cross-inoculated with 1×10^4 cells in each well into 24-well plates, and different drugs were added to each well and placed in the incubator for 1 hour for ultrasonic irradiation (ultrasonic parameter: 1 MHz, irradiation for 45s, 50% space duty ratio). Then, cells were further incubated for 5 h, the culture medium was removed, and PBS was added for continuous washing 3 times. Thereafter, 10 μmol/L DCFH-DA fluorescent dye (Beyotime, Shanghai, China) was added to each well for 200 μL, and the DCFH-DA was incubated for 30 min away from light. Cells were then washed with PBS 3 times, and 500 μL of DMEM (-) were added to each well. The fluorescence of each group was observed under an inverted fluorescence microscope.

The Targeting PD-L1 Ability on the Tumor Cells with PD-L1 mAb/DOX-NBs in vitro and in vivo

Hepa1-6 cells cultured with PD-L1 mAb/DOX-NBs or DOX-NBs were co-incubated and washed with PBS twice to remove the NBs that did not adhere to cells. Then, cells were fixed with paraformaldehyde (Servicebio, China), and nuclei were stained with 4′,6-diamidino2-phenylindole (DAPI, Servicebio, China). The targeted aggregation of NBs at the cell level was observed under an inverted fluorescence microscope.

The in vivo targeting experiment was carried out through contrast-enhanced ultrasound (CEUS) imaging. H22 tumor-bearing mice were injected with 200 μL DOX-NBs, PD-L1 mAb-NBs, and PD-L1 mAb/DOX-NBs via the tail vein. In real-time, tumor enhancement was monitored by in vitro ultrasound to evaluate the contrast imaging ability and retention of NBs in vivo. CEUS imaging was operated by Mindray RE-7 (Mindray Medical International Co., Ltd. China), equipped with an 18 MHz central frequency linear probe, and quantitative analyses were performed using Sonamath software (AmbitionT. C., China).

Pharmacokinetic Study of PD-L1 mAb/DOX-NBs

Tumor-bearing mice were injected with 200 μL DOX, DOX-NBs, and PD-L1mAb/DOX-NBs via the tail vein, with 3 mice in each group. After 24 h, the mice were sacrificed, and the tumor and various organs were stripped. The distribution and aggregation of DOX in tumors and organs were observed with an in vivo imaging system (IVIS® Lumina XRMS Series III, PerkinElmer, USA). The excitation and emission wavelengths were set to 485 and 570 nm, respectively.

The tumor tissue, after later treatment, was prepared into frozen sections and cut into 10-μm slices. Tissue sections were fixed with paraformaldehyde for 20 min, stained with DAPI for 15 min, washed with PBS 3 times, and finally sealed with an anti-fluorescence quenching agent. Fluorescence aggregation of DOX in the tumor tissues of each group was obtained under a fluorescence microscope, and fluorescence intensity was quantitatively analyzed by Image J software 1.51k (ACEA Bioscience, Inc.; Agilent Technologies, Inc.).

In vivo Antitumor Studies

The antitumor studies were carried out in H22 hepatoma tumor models. A total of 65 SPF Balb/C female mice weighing 18–20 g and aged 6–8 weeks were ordered. H22 hepatoma cells were diluted to 1×10^7/mL, and the 150 μL cell suspension was injected into the right anterior axilla of each mouse. Group therapy was started when the tumor grew to 100 mm³. Tumor-bearing mice were randomly divided into 8 groups: Control, N-NBs+US, DOX, DOX+US, PD-L1 mAb, DOX-NBs+US, PD-L1 mAb-NBs+US, PD-L1 mAb/DOX-NBs + US. Thereafter, 200 μL of normal saline, DOX solution, and NBs were injected through the tail vein, and the DOX dose was 3 mg/kg. Mice were treated once every

other day, for 6 times in total. US irradiation was conducted at the tumor site immediately after injection in the US group. The irradiation parameters were set to power: 1 W/cm^2, frequency: 1 MHz, duty cycle: 50%, and irradiation time: 120 seconds. During treatment, we measured the bodyweight and the long (a) and short (b) diameters of the tumor, and the tumor volume was calculated according to the formula $V = 1/2ab^2$.

After the last treatment, the tumors and major organs were harvested. For the survival study, we measured the tumor weight of each group, drew the tumor growth curve, and calculated the tumor inhibition rate. Tumor volume inhibition rate = (1 - experimental group tumor volume/control group tumor volume) × 100%, Tumor mass inhibition rate = (1 - The mass of the tumor in the experimental group/the mass of the tumor in the control group) × 100%.

Hematoxylin and Eosin Staining
The tumor tissue and various organs were embedded and fixed in paraffin to prepare tissue sections. After staining with hematoxylin and eosin (H&E), the morphological changes in tumor tissues and different organs were observed.

TUNEL Assay
To evaluate the apoptosis of tumor tissues, the TUNEL cell apoptosis detection kit (Meilunbio, China) was used, with green fluorescence representing apoptotic bodies. The apoptosis of tumor cells was observed under a fluorescence microscope.

Immunohistochemistry
After dewaxing, hydration, and antigen retrieval, paraffin sections of tumor tissues were incubated with 3% H_2O_2 for 30 min, to remove endogenous peroxidase, and then blocked with 5% albumin from bovine serum (BSA, Solarbio, China) for 1 h to reduce non-specific protein binding. Sections were then incubated with diluted Bax (1:200 dilution, Proteintech, Wuhan, China) and Bcl-2 antibodies (1:200 dilution, Santa Cruz, USA) overnight, and incubated with their corresponding secondary antibody for 1 h at room temperature, washed with PBS, and counterstained with hematoxylin after DAB (Biological Technology Co Ltd) color development. After washing, we sealed the slides with a neutral resin glue, and after drying, pictures were obtained and analyzed under an inverted fluorescence microscope.

Immunofluorescence
Cells or 4-μm tumor tissue slices were incubated with antibodies (PD-L1, CRT, 1:200 dilution, Proteintech, Wuhan, China; FITC-labeled CD8 antibody and PE-labeled IFN-γ antibody, BioLegend, USA) in a wet box at 4°C for 12–16 h, rinsed with PBS, and subsequently treated with a fluorescent secondary antibody for 1 h, followed by PBS washing. The expression of target proteins in the cells or tumor tissues was observed under the fluorescence microscope. Then, a quantitative analysis of target protein levels was obtained by ImageJ software analysis.

RT-qPCR
The total RNA was extracted from various tumor tissues by the trizol method, preserved at −80 °C, and reversed transcribed into cDNA with a reverse transcription kit (Vazyme Biotech Co., China). Each cDNA sample was analyzed with the Applied Biosystems the 7900HT Fast Real-Time PCR System (Applied Biosystems, Foster City, CA, USA), using the Taq Pro Universal SYBR qPCR Master Mix (Vazyme Biotech Co., China) according to the manufacturer's protocol. The thermocycling parameters were 95°C pre-denaturation for 20s, 95°C denaturation for 3 s, 60°C annealing for 30s, 72°C extension for 1 min, and 40 cycles of amplification. β-actin served as a control, and the relative expression levels of B-cell lymphoma-2-associated X (Bax), B-cell lymphoma-2 (Bcl-2), cluster of differentiation 80 (CD80), tumor necrosis factor alpha (TNF-α), and interferon gamma (IFN-γ) were evaluated by the $^{-2\Delta\Delta}$Ct method. The primers used in RT-qPCR are shown in Table 1.

Western Blotting
The tumor tissues of each group were lysed, and total protein was extracted. After quantification with the bicinchoninic acid assay (BCA kit; Boster, Wuhan, China), the protein loading buffer was added and boiled in boiling water for 10 min.

Table 1 Primer Sequences for Gene

Gene	Primer	Sequences
β-actin	Sense Antisense	GGAGATTACTGCCCTGGCTCCTA GACTCATCGTACTCCTGCTTGCTG
Bax	Sense Antisense	TGGTTGCCCTCTTCTACTTTGC CAGACAAGCAGCCGCTCAC
Bcl-2	Sense Antisense	CGTCAACAGGGAGATGTCACC CAGCCAGGAGAAATCAAACAGAG
TNF-α	Sense Antisense	TCAACCTCCTCTCTGCCGTC GAGCAATGACTCCAAAGTAGACCTG
CD80	Sense Antisense	TCTCCACGGAAACAGCATCT CTTACGGAAGCACCCATGAT
IFN-γ	Sense Antisense	CCATCGGCTGACCTAGAGAA GATGCAGTGTGTAGCGTTCA

Abbreviations: β-actin, beta-actin; Bax, B-cell lymphoma-2-associated X; Bcl-2, B-cell lymphoma-2; TNF-α, tumor necrosis factor alpha; CD80, cluster of differentiation 80; IFN-γ, interferon gamma.

After 2 h of SDS-PAGE gel electrophoresis, the protein was transferred to the PVDF membrane using a wet transfer method for 1.5 h. The membrane was blocked with 5% skimmed milk for 1 h, and incubated with rabbit polyclonal HMGB1 antibody (1:500 dilution, Wanleibio, Shenyang, China) overnight on a 4°C shaker. The membrane was then washed 3 times with TBST for 10 min each time and incubated with HRP-labeled goat anti-rabbit IgG (1:4000 dilution) at room temperature for 1 hour. The membrane was washed with TBST 3 times, 10 min each time, and an ECL chemiluminescence developing solution (Servicebio, China) was used for signal detection. β-actin served as an internal control.

Flow Cytometry

The spleens of each group were stripped, and the spleen cell suspension was prepared after grinding, with 3 spleens in each group. The cell suspensions of each group were incubated with fluorescent dye CFDA-SE (Meilunbio, China) for 30 minutes and then inoculated into 24-well plates. The tumor antigen was added to each well. Well plates were incubated at 5% CO_2 and 37°C for 48 h. Then, the spleens of each group were collected, washed with PBS 3 times, centrifuged at 1500 rpm for 5 min, and the proliferation of splenic lymphocytes was detected by flow cytometry.

An appropriate amount of diluted PE-labeled anti-mouse NK1.1 antibody (Biolegend, USA) was added to the spleen lymphocytes in each group and incubated in the dark for 30 minutes. After centrifugation and washing 3 times, the proportion of natural killer (NK) cells was detected by flow cytometry. Then, diluted FITC and APC-labeled anti-mouse CD3 and CD8 antibodies (Biolegend, USA) were added to double-strain spleen lymphocytes. Flow cytometry detected the proportion of cytotoxic T lymphocytes (CTLs) after centrifugation and washing 3 times.

LDH Release Assay

The treated and cultured spleen cells were counted and inoculated into 96-well plates at 1×10^7 cells per well. The spleen lymphocytes prepared above were stimulated by the specific tumor antigen (1 μg/mL) for the CTL assay. Splenic lymphocytes were used as effector cells, and H22 hepatoma cells were used as target cells. The effector and target cells were added to the experimental group according to the effect target ratio of 50:1. Cells were co-cultivated for 4 hours, and a set blank control group, natural release group, and maximum release group were simultaneously set. The LDH Assay Kit (Beyotime, Shanghai, China) was used to detect the in vitro killing activity of NK cells against H22 liver cancer cells.

The absorbance of each well was measured at 490 nm with a microplate reader. Killing rate = (absorbance of experimental group - absorbance of natural release group)/(absorbance of maximum release group - absorbance of natural release group) × 100%.

Statistical Analysis

SPSS 18.0 (SPSS Inc., Chicago, USA) and Prism (Graphpad V6.0) were used for statistical analyses of the experimental data. Data were expressed as mean ± SD. The Student's *t*-test and one-way analysis of variance (ANOVA) were used to compare two and multiple groups. *P* values<0.05 were considered statistically significant.

Results

Characterization of PD-L1 mAb/DOX-NBs

We prepared the PD-L1mAb/DOX-NBs as shown in Figure 1A–F.The NB suspension was red in appearance and, as observed under a fluorescence microscope, displayed spontaneous red fluorescence, good dispersion, and no apparent adhesion and aggregation.(Figure 1C). Scanning electron microscopy (SEM) showed that the NBs were spherical, and their shell was smooth and complete (Figure 1B). The average particle size was 457.1 ± 23.2 nm (Figure 1D). The drug encapsulation rate of DOX in PD-L1mAb/DOX-NBs was 43.65 ± 3.84% by the thin-film dialysis method, indicating that NBs successfully encapsulated DOX.

By introducing the bridged avidin-biotin (BRAB) technique, both biotinylated NBs and the biotinylated PD-L1 antibody were cross-linked through avidin to prepare PD-L1mAb/DOX-NBs, which were observed under a confocal laser scanning microscope (CLSM). The results showed the merged yellow spot images from the red fluorescence of biotinylated DOX-NBs and green fluorescence of FITC-labeled biotinylated PD-L1 antibody, indicating that the PD-L1 antibody was successfully conjugated to the surface of the biotinylated DOX-NBs (Figure 1E). Flow cytometry was used further to identify the binding rate between DOX-NBs and the PD-L1 antibody, which was 72.85 ± 13.56% (Figure 1F).

Pharmacokinetic Analysis and Tissue Distribution of PD-L1 mAb/DOX-NBs

To investigate the tissue distribution of DOX or the NBs, which were injected into tumor-bearing mice via tail vein, the tumors and organs were observed through DOX fluorescence by in vivo imaging using the small animal imaging system IVIS®. DOX was mainly concentrated in tumor sites, followed by the liver and kidney, suggesting that it may be metabolized by them (Figures 2A and C). The intratumor fluorescence intensities in the DOX-NB group and the PD-L1 mAb/DOX-NB group were 2.5 times and 3.5 times higher than that in the DOX group, respectively, indicating that NBs can increase the concentration of DOX in the tumor site, and that the aggregation effect of PD-L1 mAb/DOX-NBs is better (Figure 2C, *P* < 0.05).

Additionally, a frozen section of the tumor tissues showed that only a small amount of DOX was collected in the tumor cytoplasm in the DOX group. At the same time, DOX was more enriched in the tumor cytoplasm in the DOX-NB and PD-L1mAb/DOX-NB groups, and the aggregation effect was the highest in the PD-L1 mAb/DOX-NB group (Figures 2D and F). It was further demonstrated that PD-L1mAb/DOX-NBs could enhance DOX concentrations at the tumor site, suggesting that targeted NBs can be used as a suitable delivery carrier for DOX to improve its antitumor effect.

NBs were injected into the tumor-bearing mice through the tail vein and tumors were observed by CEUS imaging. All three types of NBs had good contrast imaging capabilities in vivo (Figure 2B). However, after the injection of DOX-NBs for 150 s, the contrast agent in the tumor disappeared. At the same time, there was still some contrast agent in the tumor of PD-L1 mAb-NBs and PD-L1 mAb/DOX-NBs, indicating that targeted NBs may display specific aggregation at the transplanted tumor site of mice and can prolong their retention time (Figures 2B and E).

To further verify that PD-L1 mAb/DOX-NBs target PD-L1 on the tumor cells, firstly, the expression of PD-L1 on the surface of Hepa1-6 cells was detected by the immunofluorescence method. We observed strong green fluorescence on the surface of Hepa1-6 cells, indicating high PD-L1 expression in liver cancer cells (Figure 2G).
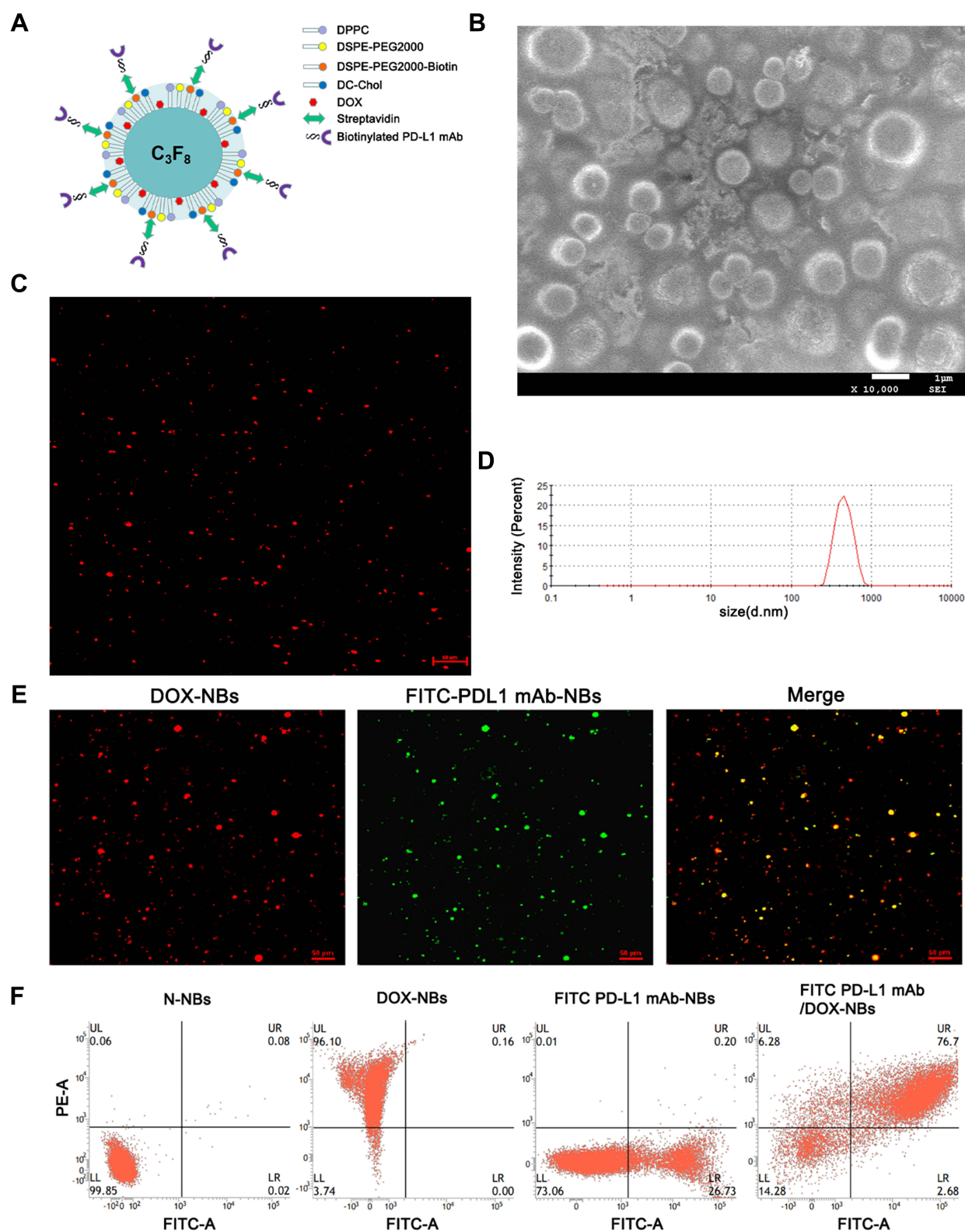
Figure I Characterization of PD-L1 mAb/DOX-NBs. (**A**) PD-L1 mAb/DOX-NBs structure model diagram. (**B**) Morphology images captured by SEM (10,000×, scale bar = 1 μm. (**C**) Morphological characteristics under a fluorescence microscope (200×, scale bar = 50 μm). (**D**) Particle size of PD-L1 mAb/DOX-NBs. (**E**) Identification of PD-L1 mAb/DOX-NBs antibody ligation under CLSM (600×). (**F**) The antibody binding rate was detected by flow cytometry.
Abbreviations: PD-L1, programmed death-ligand 1; PD-L1 mAb, PD-L1 monoclonal antibody; DOX, doxorubicin; NBs, nanobubbles; SEM, scanning electron microscope; CLSM, confocal laser scanning microscopy.
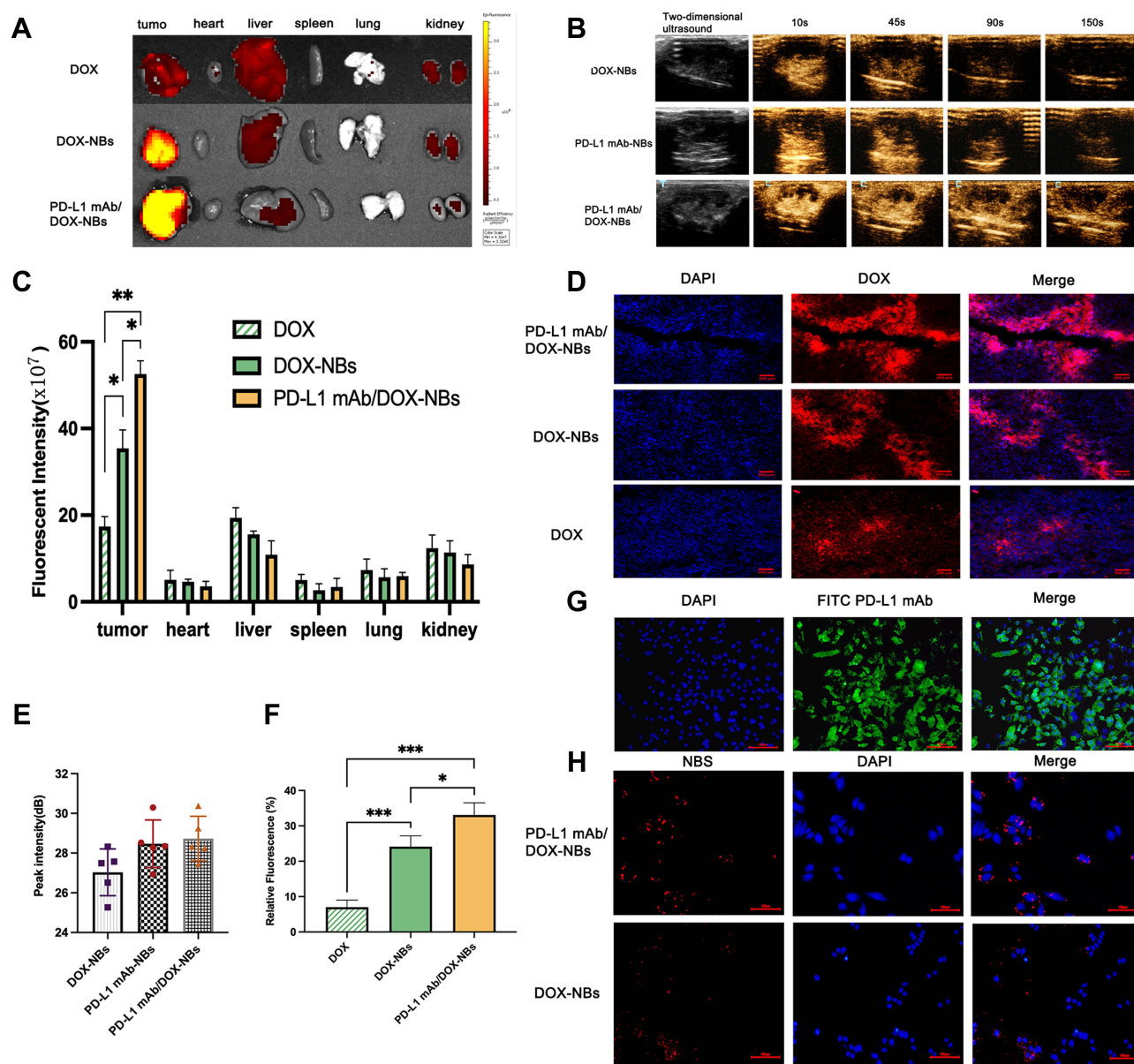
Figure 2 Biodistribution and pharmacokinetic profiles of PD-L1 mAb/DOX-NBs. (**A**) The distribution of PD-L1 mAb/DOX-NBs in tumors and organs was observed by IVIS. (**B**) The results of contrast-enhanced ultrasound (CEUS) imaging showed that PD-L1mAb/DOX-NBs enhanced imaging and in vivo targeted detection. The peak intensity (**E**) of CEUS in vivo showed no significant differences among the groups. (**C**) Quantitative analysis of fluorescence intensity of tumors and organs shown in (**A**). (**D**) The enrichment of DOX in tumor sites was observed by frozen sections (200×, scale bar = 200 μm). (**F**) Quantitative analysis of the relative fluorescence of DOX shown in (**D**). (**G**) Cellular immunofluorescence detection of PD-L1 expression on the surface of Hepa1-6 cells. Green fluorescence represents the highly expressed PD-L1 protein on the surface of Hepa1-6 cells (200×, scale bar = 100 μm). (**H**) In vitro targeting detection of PD-L1 mAb/DOX-NBs (200×, scale bar = 100 μm). *$P < 0.05$, **$P < 0.01$, ***$P < 0.001$.
Abbreviations: PD-L1, programmed death-ligand 1; PD-L1 mAb, PD-L1 monoclonal antibody; DOX, doxorubicin; NBs, nanobubbles; CEUS, contrast-enhanced ultrasound imaging.

After co-incubation of PD-L1 mAb/DOX-NBs or DOX-NBs with Hepa1-6 hepatoma cells, fluorescence microscopy results showed that PD-L1 mAb/DOX-NBs were specifically bound to hepatoma cells. In contrast, DOX-NBs showed no apparent adhesion around hepatoma cells. These results indicate that targeted NBs have specific aggregation and targeting ability in vitro and actively target liver cancer cells (Figure 2H).

Tumor Inhibition Effects of PD-L1 mAb/DOX-NBs in a Transplanted Tumor Mouse Model

The antitumor performance of PD-L1 mAb/DOX-NBs was assessed in H22 tumor-bearing mice, and the antitumor treatment process is shown in Figure 3A. The corresponding growth curve is shown in Figure 3B. The transplanted tumor
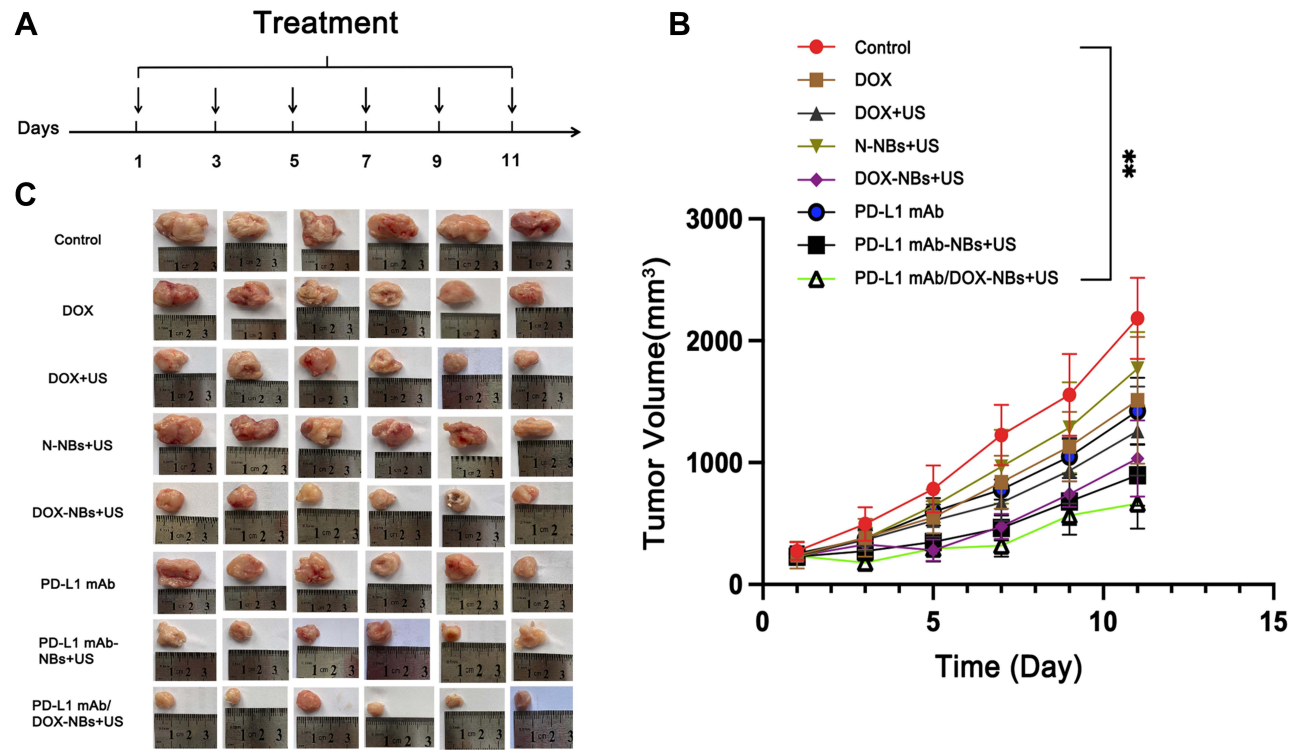
Figure 3 In vivo experiment of PD-L1 mAb/DOX-NBs against liver cancer subcutaneous transplantation. (**A**) In vivo experimental treatment plan. (**B**) Tumor growth curve of each group. (**C**) Comparison of tumor size in each group.
Abbreviations: PD-L1, programmed death-ligand 1; PD-L1 mAb, PD-L1 monoclonal antibody; DOX, doxorubicin; NBs, nanobubbles.

volume gradually increased during treatment, especially in the control group. The size of various tumors is shown in Figure 3C. Compared with the control group, tumor volume and mass growth in all treatment groups were inhibited, and the PD-L1 mAb/DOX-NBs+US group had the most significant inhibitory efficiency (Figure 3 and Table 2).

Table 2 Tumor Inhibition Rate of Tumor Volume and Weight in Each Group

Groups	Tumor Volume (mm³)	Tumor Weight (g)	Volume Inhibition Rate (%)	Weight Inhibition Rate (%)
Control	2184.84 ± 333.6	3.05 ± 0.74	0	0
DOX	1511.93 ± 521.5	2.14 ± 0.55	30.30*	29.92*
DOX+US	1259.36 ± 364.7	1.66 ± 0.47	42.36**	45.60**
N-NBs+US	1772.48 ± 300.1	2.54 ± 0.55	18.87	16.93
DOX-NBs+US	1033.89 ± 313.7	1.34 ± 0.22	52.68**	56.20**
PD-L1 mAb	1423.28 ± 273.4	1.94 ± 0.58	33.43*	36.48*
PD-L1 mAb-NBs+US	895.91 ± 250.8	1.11 ± 0.23	58.99**	63.63**
PD-L1 mAb/ DOX-NBs+US	663.42 ± 204.7	0.73 ± 0.16	69.64**	75.97**

Notes: * $P < 0.05$, **$P < 0.01$ vs with control group.
Abbreviations: DOX, doxorubicin; US, ultrasound; NBs, nanobubbles; PD-L1, programmed death-ligand 1; PD-L1 mAb, PD-L1 monoclonal antibody.

PD-L1mAb/DOX-NBs Induce Tumor Cell Apoptosis

To evaluate the antitumor activity of PD-L1 mAb/DOX-NBs, H&E staining was used to detect the histopathological changes in tumor tissue and a TUNEL assay was used to observe cell apoptosis levels. H&E staining revealed that different degrees of degeneration and necrosis in all treatment groups, especially in the PD-L1 mAb/DOX-NBs+US group (Figure 4A). In contrast, the cells in the control group proliferated actively, their nuclei were large and hyperchromatic, their nucleocytoplasmic ratio was increased, and they showed significant atypia. The percentage of apoptotic cells in the DOX group was increased compared with that in the control ($P < 0.05$) (Figures 4B and D). We designed another control group, DOX-NBs+US, which had a higher percentage of apoptotic cells than that in DOX+US and NBs+US ($P < 0.05$). Finally, we prepared PD-L1 mAb/DOX-NBs+US to treat the tumor, in which the percentage
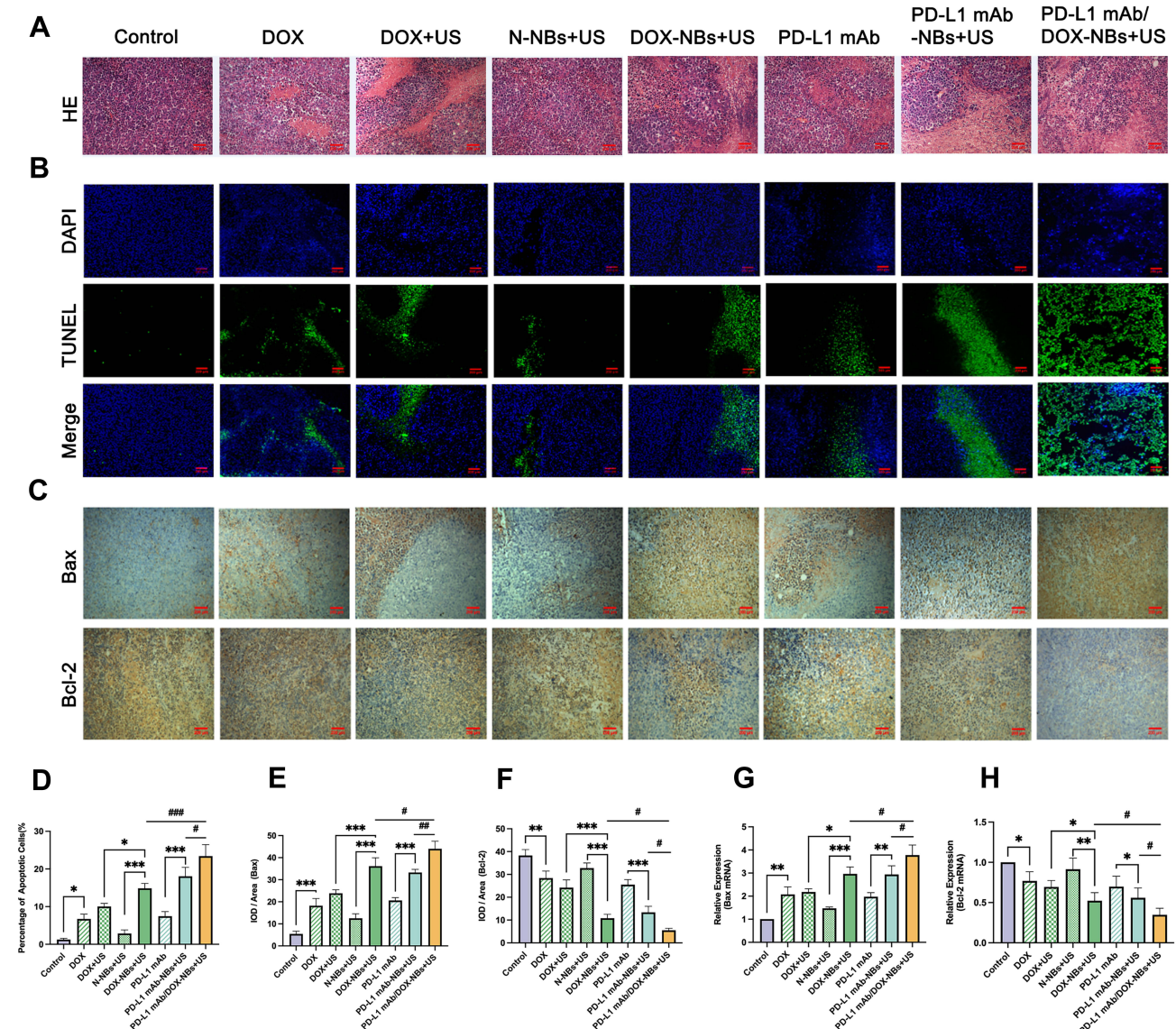

Figure 4 Antitumor activity analysis of PD-L1 mAb/DOX-NBs. (**A**) HE staining was used to observe morphological changes of tumor tissues in each group (200×, scale bar = 200 μm). (**B**) Apoptosis of tumor tissues was detected by TUNEL. (**C**) Immunohistochemistry was used to detect Bax and Bcl-2 protein expression levels in tumor tissues (200×, scale bar = 200 μm). (**D**) Semi-quantification of the fluorescence intensity shown in (**B**). (**E**) and (**F**) Semi-quantitative analysis of immunohistochemistry results shown in (**C**). (**G**) and (**H**) The mRNA expression levels of Bax and Bcl-2 in tumor tissues, detected by RT-qPCR. *$P < 0.05$, **$P < 0.01$, ***$P < 0.001$, #$P < 0.05$, ##$P < 0.01$, ###$P < 0.001$.
Abbreviations: PD-L1, programmed death-ligand 1; PD-L1 mAb, PD-L1 monoclonal antibody; DOX, doxorubicin; NBs, nanobubbles; HE, Hematoxylin and Eosin Staining; Bax, B-cell lymphoma-2-associated X; Bcl-2, B-cell lymphoma-2.

of apoptotic cells was higher than that in PD-L1 mAb, PD-L1 mAb-NBs+US, and DOX-NBs+US ($P < 0.05$) (Figure 4D).

Since we discovered that ultrasound-mediated PD-L1 mAb/DOX-NBs could promote the apoptosis of tumor cells, their role in regulating apoptosis-related proteins was further investigated. Bax and Bcl-2 have been found to commit a cell to its programmed death.[27] Therefore, we detected their expression in tumor cells to further investigate the antitumor activity of PD-L1 mAb/DOX-NBs. As shown in Figures 4C and E, Bax protein expression in the DOX group was increased compared with that in the control ($P < 0.001$), and that in DOX-NBs+US was yet higher than those in DOX+US and NBs+US ($P < 0.001$). The blockage of the PD1/PD-L1 pathway showed a substantial effect on inducing the upregulation of Bax and the downregulation of Bcl-2.[28] Therefore, we designed a group of PD-L1 mAb-NBs+US in which Bax protein expression was higher than that in the control and PD-L1 mAb groups ($P < 0.001$). Most importantly, that in the PD-L1 mAb/DOX-NBs+US was the highest in all the groups (Figure 4E, $P < 0.05$). However, Bcl-2 protein expression in tumor cells of each group showed the opposite result. The results of RT-qPCR showed that the gene expression of Bax and Bcl-2 corresponded to the protein expression pattern (Figures 4G and H). These results indicated that PD-L1mAb/DOX-NB-mediated combination therapy has a synergistic antitumor efficiency.

DOX Induces Tumor Immunogenic Cell Death

Previous studies have reported that DOX-triggered oxidative stress could cause the intracellular redox imbalance, contributing to the immunogenic cell death (ICD) response.[29] ROS are a significant indicator of cellular oxidative stress damage. DCFH-DA is a general indicator of oxidative stress that can detect the level of intracellular ROS production. The hepatoma cells in the DOX and DOX+US groups produced more negligible green fluorescence than those in DOX-NBs+US and PD-L1 mAb/DOX-NBs+US groups, which had a large amount of green fluorescence (Figure 5A), suggesting that ultrasound combined with NBs can enhance the DOX-induced oxidative stress injury of tumor cells and thus enhance the effect of SDT.

CRT exposure on the cell surface is one of the key markers determining chemotherapeutic agent immunogenicity. Previous studies have shown that CRT is exposed on the cell surface during the pre-apoptotic death phase and triggers DCs of the tumor environment to phagocytose dead tumor cells.[30] To assess the potential of DOX to induce ICD, we determined the CRT expression on the surface of hepatoma cells at different DOX concentrations by flow cytometry. CRT expression levels increased gradually with increasing DOX concentrations (Figure 5B), and there was a certain dose-response relationship (Figure 5E, $P < 0.01$), suggesting that DOX could promote CRT evagination exposure to the HCC cell membrane. We then used immunofluorescence to observe whether CRT could evaginate to the surface of tumor cells. As shown in Figure 5C, DOX, DOX+US, DOX-NBs+US, and PD-L1 mAb/DOX-NBs+US could promote the evagination of CRT to the tumor cell membrane.

HMGB1 is a nuclear cytokine released by cells undergoing ICD. The immunogenic characteristics of ICD are mainly mediated by DAMPs, which include surface-exposed CRT, secreted ATP, and released HMGB1.[31] Therefore, we measured the protein expression levels of HMGB1 by Western blotting. As Figures 5D and F show, DOX, DOX-NBs +US, and PD-L1 mAb/DOX-NBs+US all induced an obvious extracellular release of HMGB1. These results further validated our hypothesis that ultrasound-mediated PD-L1 mAb/DOX-NBs could cause the ICD of tumor cells.

ICD is characterized by the release of membrane-bound and soluble factors that boost the function of immune cells, such as NK cells. Cytokines such as TNF play a crucial role in creating an immunogenic microenvironment and are key players combating tumors.[32] We used flow cytometry to detect the proportion of NK cells in mouse splenic lymphocytes. Compared with that in the control group, the proportion of NK cells in the DOX group was increased (Figure 6B, $P < 0.05$). DOX-NBs+US showed a higher percentage of NK cells compared to those in DOX+US and NBs+US ($P < 0.05$). Finally, we prepared PD-L1 mAb/DOX-NBs+US, in which the percentage of NK cells was higher than that in PD-L1 mAb, PD-L1 mAb -NBs+US, and DOX-NBs+US ($P < 0.05$) (Figure 6B). The cytotoxicity of NK cells was detected through co-culture with tumor cells, which were attacked by effector cells, and rapidly released a stable cytoplasmic enzyme, LDH, tested by the LDH release assay. As shown in Figure 6C, a similar trend was observed to that in Figure 6B, indicating that PD-L1 mAb/DOX-NBs+US had the most significant effect in activating NK cells (Figure 6C, $P < 0.05$).
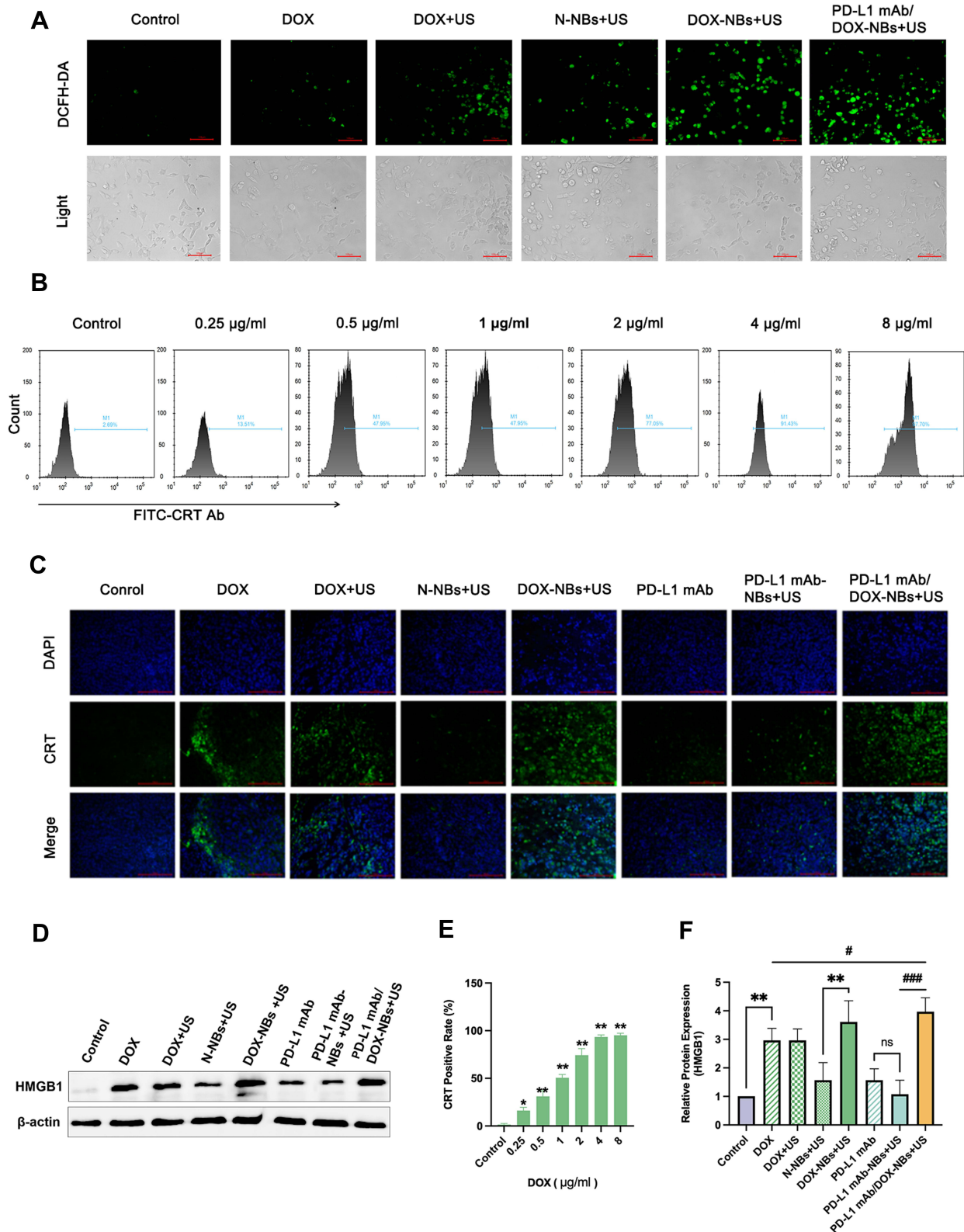
Figure 5 Antitumor mechanism of DOX-mediated sonodynamic therapy and immunotherapy. (**A**) The effect of DOX on the content of ROS in Hepa1-6 cells (200×, scale bar = 100 μm). (**B**) Effects of different concentrations of DOX on the expression of CRT on the surface of Hepa1-6 cells. (**C**) The effect of DOX on CRT expression on the tumor cell surface was detected by immunofluorescence (400×, scale bar = 100 μm). (**D**) Western blotting detected the release of HMGB1 in the tumor tissues of each group. (**E**) The expression of CRT shown in (**B**). (**F**) Quantitative analysis of Western-blot results shown in (**D**). *$P < 0.05$, **$P < 0.01$, #$P < 0.05$, ##$P < 0.01$, ###$P < 0.001$.
Abbreviations: DOX, doxorubicin; ROS, reactive oxygen species; CRT, calreticulin; HMGB1, high mobility group box B1.
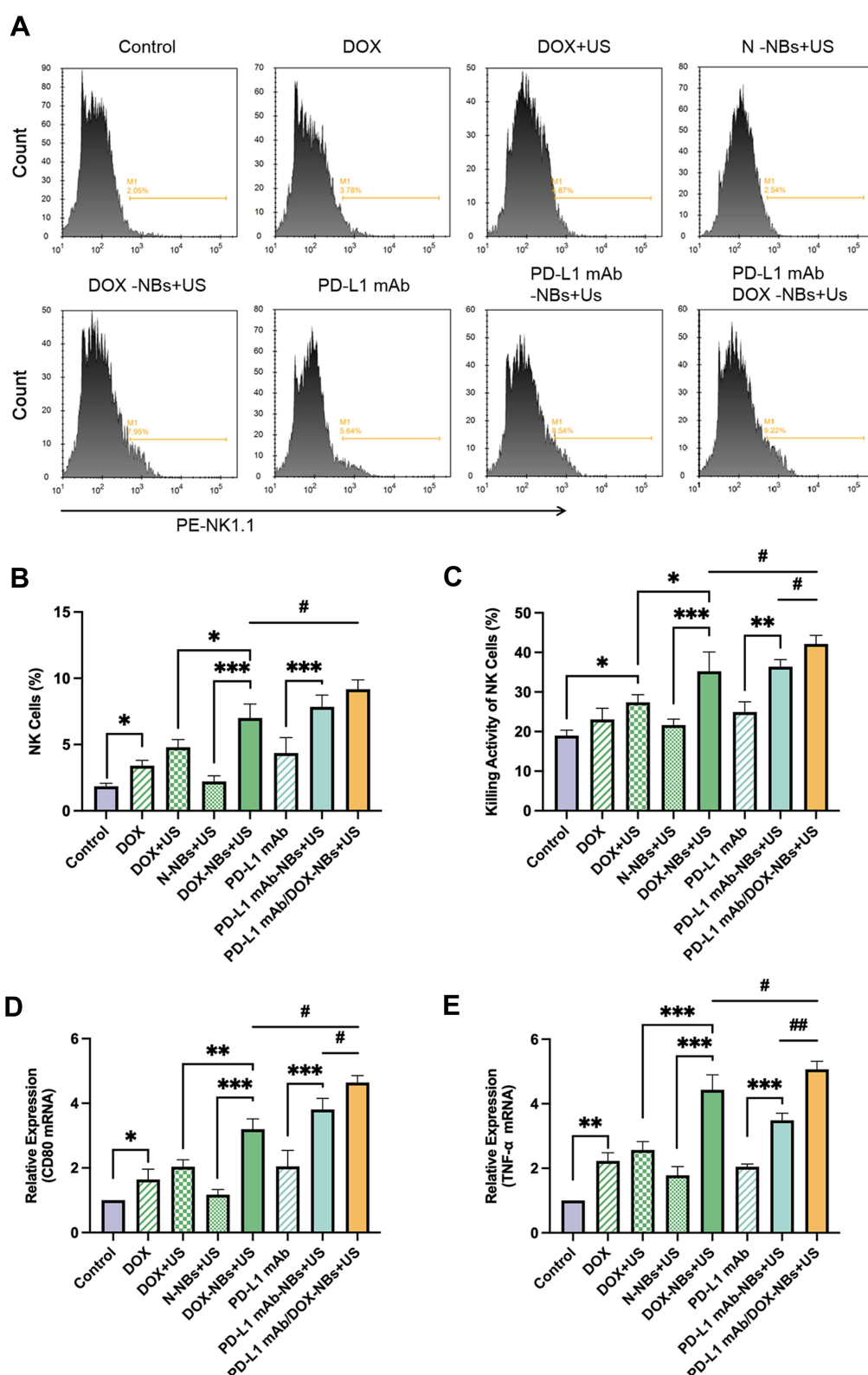
Figure 6 Mechanisms underlying the superior antitumor efficacy of PD-L1 mAb/DOX-NBs. (**A**) The proportion of NK cells in each group was detected by flow cytometry. (**B**) Quantitative analysis of the proportion of NK cells in each group. (**C**) In vitro cytotoxicity of NK cells was detected by the LDH release assay. (**D**) and (**E**) mRNA expression of CD80 and TNF-α in tumor tissues. *$P < 0.05$, **$P < 0.01$, ***$P < 0.001$, #$P < 0.05$, ##$P < 0.01$.

Abbreviations: PD-L1, programmed death-ligand 1; PD-L1 mAb, PD-L1 monoclonal antibody; DOX, doxorubicin; NBs, nanobubbles; NK, Natural Killer; LDH, lactate dehydrogenase; CD80, cluster of differentiation 80; TNF-α, tumor necrosis factor-alpha.

To further explore ICD antitumor immune activity, we examined CD80 and TNF-α expression by RT-qPCR. The mRNA expression levels of CD80 and TNF-α in the DOX group increased about 1~2 times compared to those in the control group ($P < 0.05$). The increase in the DOX-NBs+US group was significantly higher than that in DOX+US and NBs +US ($P < 0.01$). Similarly, the mRNA expression of CD80 and TNF-α in PD-L1 mAb/DOX-NBs+US showed a dramatic increase over that in the PD-L1 mAb, PD-L1 mAb -NBs+US, and DOX-NBs+US ($P < 0.05$) (Figures 6D and E).

Immune Checkpoint Inhibitor PD-L1 mAb/DOX-NBs Mediate Antitumor Immune Activity

To further investigate the antitumor activity of the immune checkpoint inhibitor PD-L1 mAb, we detected the proliferation of spleen lymphocytes by flow cytometry. Fluorescent probe CFDA-SE was used to label splenic lymphocytes catalyzed by lactase and decomposed in the form of CFSE. With cell division and proliferation, the fluorescent markers were evenly distributed to the two progenies, resulting in a two-fold decrease in their fluorescence intensity. Then, the proliferation activity of lymphocytes in vitro was detected by flow cytometry. As shown in Figures 7A and E, a tendency toward a higher activity was seen in the DOX group compared with the control ($P < 0.05$). The DOX-NBs+US group had significant proliferation, and the proliferation index in vitro increased than the DOX+US and N-NBs+US ($P < 0.001$). The PD-L1 mAb/DOX-NBs+US group showed a significantly increased active proliferation in vitro compared to PD-L1 mAb, PD-L1 mAb-NBs+US, and DOX-NBs+US ($P < 0.01$) (Figures 7A and E). The proportion of CD3+CD8+ T cells in mouse splenic lymphocytes was also analyzed by flow cytometry. CD3+CD8+ T cells in PDL1 mAb/DOX-NBs+US had the same trends as the above proliferation index (Figures 7B and F). Then the cytotoxicity of CTLs was detected by the LDH release assay, whereby tumor antigen-activated T lymphocytes co-cultured with tumor cells and the cell supernatant were collected and analyzed. The LDH results (Figure 7G) showed a similar trend to those of flow cytometry (Figure 7F).

Using immunofluorescence staining, the expressions of CD8 and IFN-γ were detected in tumor tissues. CD8 and IFN-γ protein expressions were significantly increased in the DOX group compared to those in the control group. The increase was most apparent in the PD-L1 mAb/DOX-NBs+US group, which was consistent with the trend of other indexes shown above (Figure 7C, D and H, I). The mRNA expression of IFN-γ was similar to its protein expression (Figure 7J). The above results suggested that ultrasound-mediated PD-L1 mAb/DOX-NBs have a great antitumor immunity ability, exerted by blocking the PD1/PD-L1 pathway to activate CTLs.

Discussion

As a safe and targeted tumor diagnosis and treatment method, the ultrasound NB drug delivery system has attracted considerable attention in the field of biomedicine. Ultrasound can not only monitor tumor imaging in real-time but also trigger the release of targeted drugs accurately and on-demand so that drugs can be concentrated in the target tissue, effectively prolonging the local retention time of drugs. This significantly improves treatment efficiency and reduces systemic toxicity and drug side effects, rendering it the tumor-targeted therapy strategy with the most promising potential at present.[33–35] In this study, ultrasound NBs were used as drug delivery carriers. Based on the bridging effect between biotin-streptavidin, PD-L1 mAb/DOX-NBs were successfully prepared with a small and uniform particle size, high antibody connection rate, and good safety in vivo. The advantage of the targeted NBs prepared for this work is that they have a small particle size, can penetrate the blood vessel wall and enter the tumor tissue, and have a more apparent visualization effect at the tumor site. In addition, the nanosize of NBs can also lead to their passive aggregation at the tumor site due to the EPR effect.[24]

The PD-L1 mAb attached to the surface of NBs can selectively bind to PD-L1, a specific marker of tumor cells, while combining with targeted irradiation by in vitro ultrasound to burst the NBs at the target area, thus achieving the goal of targeted therapy. The PD-L1-targeted microbubbles prepared by our group in the early stage have shown good targeting aggregation and antitumor effects.[36,37] Ultrasound-triggered, microbubble-targeted drug delivery can not only increase drug accumulation in tumors and prolong their retention time but also limit drug uptake in normal tissues, thereby reducing systemic toxicity and drug side effects.[38] Additionally, ultrasound irradiation enhanced cellular uptake and increased drug accumulation at the tumor site by 1.85-fold.[39] The VEGFR1- and FSHR-targeting microbubbles prepared
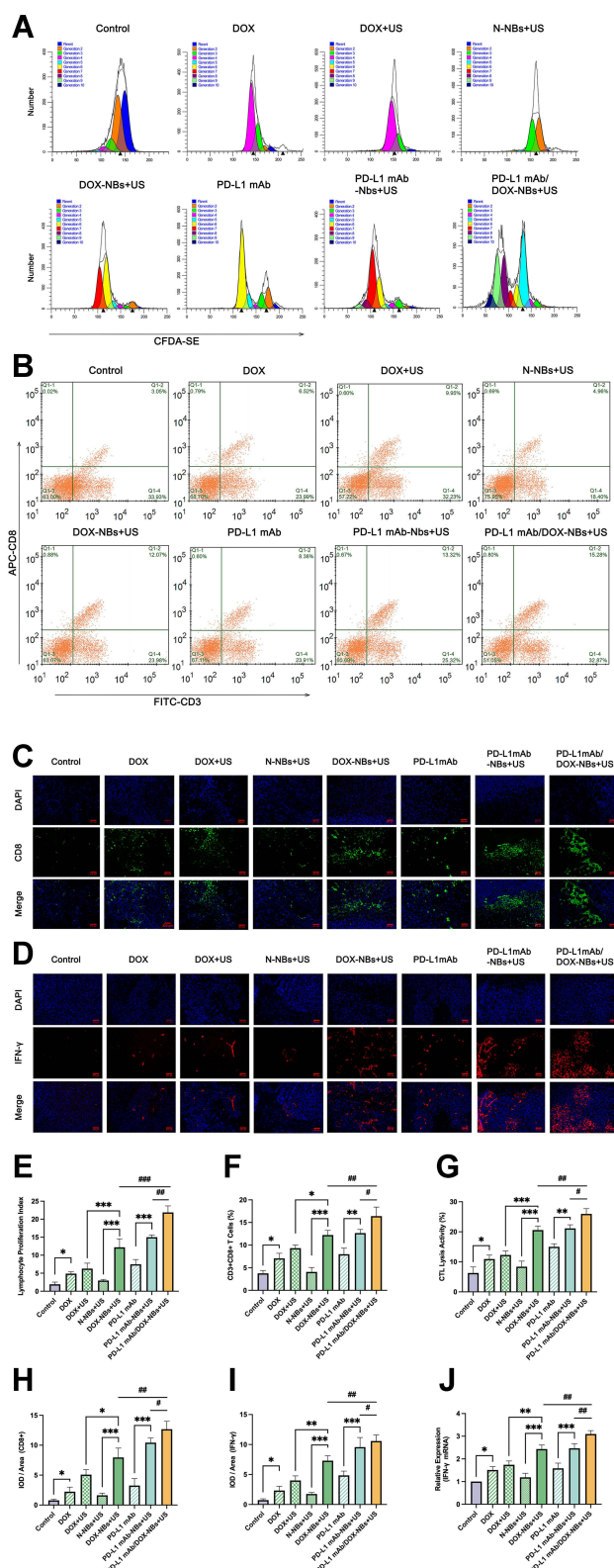
Figure 7 The mechanism of antitumor immune activity of PD-L1 mAb/DOX-NBs. (**A**) The proliferation activity of spleen lymphocytes in each group was detected by flow cytometry in vitro. (**B**) The proportion of CTL cells in each group was detected by flow cytometry. (**C**) CD8+ T cell infiltration in tumor tissue was detected by immunofluorescence (200×, scale bar = 200 μm). (**D**) IFN-γ infiltration in tumor tissue was detected by immunofluorescence (200×, scale bar = 200 μm). (**E**) Proliferation index in each group shown in (**A**). (**F**) Quantitative analysis of the proportion of CTL cells in each group shown in (**B**). (**G**) In vitro cytotoxicity of CTL cells was detected by the LDH release assay. (**H**) Quantitative analysis of CD8 expression. (**I**) Quantitative analysis of IFN-γ expression. (**J**) mRNA expression of IFN-γ in tumor tissues. *P < 0.05, **P < 0.01, ***P < 0.001, #P < 0.05, ###P < 0.01,####P < 0.001.
Abbreviations: PD-L1, programmed death-ligand 1; PD-L1 mAb, PD-L1 monoclonal antibody; DOX, doxorubicin; NBs, nanobubbles; CTL, cytotoxic T cells; IFN-γ, interferon-gamma; LDH, lactate dehydrogenase.

by Ingels et al[40] were also used for ultrasound molecular imaging of renal cell carcinoma, and the signal enhancement could be quantitatively analyzed and compared. Therefore, targeted NBs have many advantages, such as solid targeting, good safety, and integration of diagnosis and treatment, and can be used as suitable drug delivery carriers.

In the tumor microenvironment, tumors utilize a wide range of immune escape mechanisms to evade immune destruction, including the induction of an immunosuppressive microenvironment and suppression of the effector functions of CTLs. Immune checkpoint inhibitors have become a mainstay of standard cancer treatments by targeting a dysfunctional immune system and inducing CD8+ T cells to kill cancer cells. PD-1/PD-L1-targeted therapy targeting immune checkpoints induces immune-mediated tumor eradication by blocking ligand-receptor binding, restoring effector T cell function, and reversing immune suppression.[41] Ultrasound targeted microbubble destruction combined with PD-L1 blockade can promote the activation and differentiation of CD8+ T cells, increase IFN-γ secretion, reverse an immuno-suppressive microenvironment, enhance acquired immunity, and inhibit tumor growth.[42] Kim et al[43] developed a PD-L1 targeted immune microbubble complex that can not only reduce the immune-related toxicity induced by antibodies but also improve the therapeutic efficacy when combined with focused ultrasound. In addition, Li et al[44] found that the ultrasound stimulation of microbubble cavitation could promote tumor blood perfusion, enhance CD8+ T cell infiltration, and PD-L1 antibody delivery, thereby increasing the number and activity of CD8+ T cells and thus generating strong antitumor effects.

DOX not only kills cancer cells through its direct cytotoxic effects but also increases tumor immunogenicity and induces an antitumor immune response.[45] Huang et al[46] found that the combination of SDT and immunotherapy can effectively promote tumor infiltration and the activation of CTLs, resulting in anti-cancer solid immunity and long-term immune memory and thereby effectively inhibiting tumor growth and preventing postoperative recurrence. This study found that DOX can promote not only ROS production but also the release of CRT and HMGB1 in tumor cells stimulated by ultrasound, which can activate the body's immune system by enhancing ICD, thus producing strong immune killing activity.[47]

Here, the inhibitory effect of PD-L1 mAb/DOX-NBs on subcutaneously transplanted hepatocellular carcinoma was evaluated by drawing the tumor growth curve of each group, comparing the tumor size, and calculating the average tumor inhibition rate. Compared with the control group, the growth of tumor tissue in each treatment group was relatively slow, and different degrees of tumor growth inhibition were seen. The PD-L1 mAb/DOX-NBs group had the most apparent tumor inhibition effect. Antitumor activity analysis showed that different degrees of necrosis and apoptosis were observed in each treatment group. The expression of apoptosis-related genes and Bax protein increased in each treatment group, while the expression of Bcl-2 decreased. The above results showed that the PD-L1 mAb/DOX-NB group had the highest antitumor efficiency. These results indicate that PD-L1 mAb combined with DOX-NBs can further promote tumor tissue and cell apoptosis and better regulate the expression of apoptosis-related genes and proteins to play a synergistic antitumor effect. The possible reasons are as follows. First, the cavitation effect of ultrasonic NBs acts on tumor tissue and destroys tumor micro-vessels, leading to local thrombosis of the tumor, which accelerates tumor cell death. By destroying the microvascular system, which provides nutrients and oxygen to the tumor, it also inhibits tumor growth.[33] Second, after NB explosion, ultrasound fixed-point irradiation drug-loaded NBs can form many transient and reversible pores on the surface of the cell membrane. By increasing the permeability of the cell membrane, the drug can accumulate in high concentrations in the tumor, thereby enhancing its therapeutic effect. Third, the NB surface is coupled with a PD-L1 antibody with targeted recognition, which can actively target liver cancer cells with high PD-L1 expression and activate tumor-specific CTLs to kill tumor cells by blocking the PD-1/PD-L1 pathway. Gold nanoparticles conjugated with DOX and anti-PD-L1 antibodies, constructed by Emami et al,[48] have significant antitumor effects in targeted chemical photothermal therapy of colorectal cancer by combining immune checkpoint inhibitors with solid tumor chemotherapy, achieving better results than single therapy. Wang et al[49] developed a new strategy combining PD-L1 polypeptide with DOX, which can not only reduce the chemotherapy resistance of colon cancer but also enhance the immune response. Yang et al[50] designed cancer-activated DOX prodrug nanoparticles that can selectively activate ICD in cancer cells, effectively promote DC cell maturation, and increase T cell activation to induce a preferential immune response while significantly reducing DOX-related toxic side effects. In this study, PD-L1 mAb/DOX-NBs could improve the tumor immunosuppressive microenvironment and promote the activation and proliferation of T cells. It

also increased the proliferation of lymphocytes by 11-fold in vitro and the proportion of NK cells and CTL cells by about 5-fold and 4-fold, along with their killing activity in vitro by about 2-fold and 4-fold, respectively. CD8+ T cells were infiltrated in tumor tissues, the secretion of CRT and HMGB1 was increased, and the production of the immune stimulators TNF-α and IFN-γ was promoted, indicating that the combination of PD-L1 mAb, DOX-NBs, and ultrasound had a more significant antitumor immune effect.

Conclusion

The PD-L1 mAb/DOX-NBs prepared in this study have small particle sizes, and their nanosize helps them move through the capillary endothelial cell gap to the tumor, which leads to EPR effects. Meanwhile, PD-L1 mAb/DOX-NBs have well-targeting aggregation and active antitumor ability, improving DOX concentration and prolonging its retention time at the tumor site. Ultrasound-mediated PD-L1 mAb/DOX-NBs showed further enhanced targeting and controlled release properties on the local tumor. By specifically blocking the PD-1/PD-L1 pathway by PD-L1 mAb, tumor immune tolerance can be blocked, activation and effector T cell functions can be restored, and combined with DOX-induced ICD, the antitumor immune system can be further activated, which provides a potential targeted therapy strategy for HCC patients.

Acknowledgments

Disclosure

The authors report no conflicts of interest in this work.

References

1. Sung H, Ferlay J, Siegel RL., et al. Global Cancer Statistics 2020: GLOBOCAN Estimates of Incidence and Mortality Worldwide for 36 Cancers in 185 Countries. *CA Cancer J Clin*. 2021;71(3):209–249.
2. Nouri RF, Shirkhoda M, Memari F, et al. Immunotherapy a new hope for cancer treatment: a review. *Pak J Biol Sci*. 2018;21(3):135–150.
3. Kruger S, Ilmer M, Kobold S, et al. Advances in cancer immunotherapy 2019 - latest trends. *J Exp Clin Cancer Res*. 2019;38(1):268.
4. Cable J, Greenbaum B, Pe'Er D, et al. Frontiers in cancer immunotherapy-A symposium report. *Ann N Y Acad Sci*. 2021;1489(1):30–47.
5. Jiang Y, Chen M, Nie H, et al. PD-1 and PD-L1 in cancer immunotherapy: clinical implications and future considerations. *Hum Vaccin Immunother*. 2019;15(5):1111–1122.
6. Ai L, Xu A, Xu J. Roles of PD-1/PD-L1 Pathway: signaling, Cancer, and Beyond. *Adv Exp Med Biol*. 2020;1248:33–59.
7. Mocan T, Sparchez Z, Craciun R, et al. Programmed cell death protein-1 (PD-1)/programmed death-ligand-1 (PD-L1) axis in hepatocellular carcinoma: prognostic and therapeutic perspectives. *Clin Transl Oncol*. 2019;21(6):702–712.
8. Paver EC, Cooper WA, Colebatch AJ, et al. Programmed death ligand-1 (PD-L1) as a predictive marker for immunotherapy in solid tumours: a guide to immunohistochemistry implementation and interpretation. *Pathology*. 2021;53(2):141–156.
9. Motzer RJ, Penkov K, Haanen J, et al. Avelumab plus Axitinib versus Sunitinib for Advanced Renal-Cell Carcinoma. *N Engl J Med*. 2019;380 (12):1103–1115.
10. Wang J, Li J, Tang G, et al. Clinical outcomes and influencing factors of PD-1/PD-L1 in hepatocellular carcinoma. *Oncol Lett*. 2021;21(4):279.
11. Powles T, Park SH, Voog E, et al. Avelumab Maintenance Therapy for Advanced or Metastatic Urothelial Carcinoma. *N Engl J Med*. 2020;383 (13):1218–1230.
12. Herbst RS, Giaccone G, de Marinis F, et al. Atezolizumab for First-Line Treatment of PD-L1-Selected Patients with NSCLC. *N Engl J Med*. 2020;383(14):1328–1339.
13. Jiang M, Zeng J, Zhao L, et al. Chemotherapeutic drug-induced immunogenic cell death for nanomedicine-based cancer chemo-immunotherapy. *Nanoscale*. 2021;13(41):17218–17235.
14. Ahmed A, Tait S. Targeting immunogenic cell death in cancer. *Mol Oncol*. 2020;14(12):2994–3006.
15. Si Y, Yue J, Liu Z, et al. Phase-transformation nanoparticle-mediated sonodynamic therapy: an effective modality to enhance anti-tumor immune response by inducing immunogenic cell death in breast cancer. *Int J Nanomedicine*. 2021;16:1913–1926.
16. Cheng D, Wang X, Zhou X, et al. Nanosonosensitizers with ultrasound-induced reactive oxygen species generation for cancer sonodynamic immunotherapy. *Front Bioeng Biotechnol*. 2021;9:761218.
17. Teranishi R, Matsuda T, Yuba E, et al. Sonodynamic therapeutic effects of sonosensitizers with different intracellular distribution delivered by hollow nanocapsules exhibiting cytosol specific release. *Macromol Biosci*. 2019;19(4):e1800365.
18. Zhang YW, Shi J, Li YJ, Wei L. Cardiomyocyte death in doxorubicin-induced cardiotoxicity. *Arch Immunol Ther Exp (Warsz)*. 2009;57 (6):435–445.

19. Chan KH, Lee WH, Ni M, Loo Y, Hauser CAE. C-terminal residue of ultrashort peptides impacts on molecular self-assembly, hydrogelation, and interaction with small-molecule drugs. *Sci Rep*. 2018;8(1):17127.

20. Chen ZJ, Yang SC, Liu XL, et al. Nanobowl-Supported Liposomes Improve Drug Loading and Delivery. *Nano Lett*. 2020;20(6):4177–4187.

21. Yaghoubi A, Ramazani A. Anticancer DOX delivery system based on CNTs: functionalization, targeting and novel technologies. *J Control Release*. 2020;327:198–224.

22. Dwivedi P, Kiran S, Han S, et al. Magnetic Targeting and ultrasound activation of liposome-microbubble conjugate for enhanced delivery of anticancer therapies. *ACS Appl Mater Interfaces*. 2020;12(21):23737–23751.

23. Punjabi M, Xu L, Ochoa-Espinosa A, et al. Ultrasound Molecular Imaging of Atherosclerosis With Nanobodies: translatable Microbubble Targeting Murine and Human VCAM (Vascular Cell Adhesion Molecule) 1. *Arterioscler Thromb Vasc Biol*. 2019;39(12):2520–2530.

24. Subhan MA, Yalamarty S, Filipczak N, et al. Recent Advances in Tumor Targeting via EPR Effect for Cancer Treatment. *J Pers Med*. 2021;11(6):571.

25. Bressand D, Novell A, Girault A, et al. Enhancing Nab-Paclitaxel Delivery Using Microbubble-Assisted Ultrasound in a Pancreatic Cancer Model. *Mol Pharm*. 2019;16(9):3814–3822.

26. Sun L, Zhang J, Xu M, et al. Ultrasound Microbubbles Mediated Sonosensitizer and Antibody Co-delivery for Highly Efficient Synergistic Therapy on HER2-Positive Gastric Cancer. *ACS Appl Mater Interfaces*. 2022;14(1):452–463.

27. Hafezi S, Rahmani M. Targeting BCL-2 in Cancer: advances, Challenges, and Perspectives. *Cancers*. 2021;13(6):1292.

28. Liang L, Ge K, Zhang F, Ge Y. The suppressive effect of co-inhibiting PD-1 and CTLA-4 expression on H22 hepatomas in mice. *Cell Mol Biol Lett*. 2018;23:58.

29. Zhao L, Zheng R, Liu L, et al. Self-delivery oxidative stress amplifier for chemotherapy sensitized immunotherapy. *Biomaterials*. 2021;275:120970.

30. Obeid M, Tesniere A, Ghiringhelli F, et al. Calreticulin exposure dictates the immunogenicity of cancer cell death. *Nat Med*. 2007;13(1):54–61.

31. Krysko DV, Garg AD, Kaczmarek A, Krysko O, Agostinis P, Vandenabeele P. Immunogenic cell death and DAMPs in cancer therapy. *Nat Rev Cancer*. 2012;12(12):860–875.

32. Showalter A, Limaye A, Oyer JL, et al. Cytokines in immunogenic cell death: applications for cancer immunotherapy. *Cytokine*. 2017;97:123–132.

33. Li H, Zhang Y, Shu H, et al. Highlights in ultrasound-targeted microbubble destruction-mediated gene/drug delivery strategy for treatment of malignancies. *Int J Pharm*. 2021;613:121412.

34. Delaney LJ, Eisenbrey JR, Brown D, et al. Gemcitabine-loaded microbubble system for ultrasound imaging and therapy. *Acta Biomater*. 2021;130:385–394.

35. Ruan JL, Browning RJ, Yildiz YO, et al. Ultrasound-Mediated Gemcitabine Delivery Reduces the Normal-Tissue Toxicity of Chemoradiation Therapy in a Muscle-Invasive Bladder Cancer Model. *Int J Radiat Oncol Biol Phys*. 2021;109(5):1472–1482.

36. Ma Y, Han J, Jiang J, et al. Ultrasound targeting of microbubble-bound anti PD-L1 mAb to enhance anti-tumor effect of cisplatin in cervical cancer xenografts treatment. *Life Sci*. 2020;262:118565.

37. Liu Y, Jiang J, Liu C, et al. Synergistic anti-tumor effect of anti-PD-L1 antibody cationic microbubbles for delivery of the miR-34a gene combined with ultrasound on cervical carcinoma. *Am J Transl Res*. 2021;13(3):988–1005.

38. Ingram N, Mcveigh LE, Abou-Saleh RH, et al. Ultrasound-triggered therapeutic microbubbles enhance the efficacy of cytotoxic drugs by increasing circulation and tumor drug accumulation and limiting bioavailability and toxicity in normal tissues. *Theranostics*. 2020;10(24):10973–10992.

39. Chung IJ, Moon H, Jeon SI, et al. Ultrasound-triggered imaging and drug delivery using microbubble-self-aggregate complexes. *J Biomater Sci Polym Ed*. 2022;33(1):57–76.

40. Ingels A, Leguerney I, Cournède PH, et al. Ultrasound Molecular Imaging of Renal Cell Carcinoma: VEGFR targeted therapy monitored with VEGFR1 and FSHR targeted microbubbles. *Sci Rep*. 2020;10(1):7308.

41. Wang Z, Wu X. Study and analysis of antitumor resistance mechanism of PD1/PD-L1 immune checkpoint blocker. *Cancer Med*. 2020;9(21):8086–8121.

42. Tan X, Yi C, Zhang Y, et al. Ultrasound-Targeted Microbubble Destruction Alleviates Immunosuppression Induced by CD71(+) Erythroid Progenitor Cells and Promotes PDL-1 Blockade Immunotherapy in the Lewis Lung Cancer Model. *Front Oncol*. 2021;11:768222.

43. Kim D, Lee SS, Moon H, et al. PD-L1 Targeting Immune-Microbubble Complex Enhances Therapeutic Index in Murine Colon Cancer Models. *Pharmaceuticals*. 2020;14(1):6.

44. Li N, Tang J, Yang J, et al. Tumor perfusion enhancement by ultrasound stimulated microbubbles potentiates PD-L1 blockade of MC38 colon cancer in mice. *Cancer Lett*. 2021;498:121–129.

45. Han R, Liu Q, Lu Y, et al. Tumor microenvironment-responsive Ag(2) S-PAsp(DOX)-cRGDnanoparticles-mediated photochemotherapy enhances the immune response to tumor therapy. *Biomaterials*. 2022;281:121328.

46. Huang J, Xiao Z, An Y, et al. Nanodrug with dual-sensitivity to tumor microenvironment for immuno-sonodynamic anti-cancer therapy. *Biomaterials*. 2021;269:120636.

47. Abdel-Bar HM, Walters AA, Lim Y, et al. An "eat me" combinatory nano-formulation for systemic immunotherapy of solid tumors. *Theranostics*. 2021;11(18):8738–8754.

48. Emami F, Banstola A, Vatanara A, et al. Doxorubicin and Anti-PD-L1 Antibody Conjugated Gold Nanoparticles for Colorectal Cancer Photochemotherapy. *Mol Pharm*. 2019;16(3):1184–1199.

49. Wang M, Shu XS, Li M, et al. A Novel Strategy Conjugating PD-L1 Polypeptide With Doxorubicin Alleviates Chemotherapeutic Resistance and Enhances Immune Response in Colon Cancer. *Front Oncol*. 2021;11:737323.

50. Yang S, Shim MK, Kim WJ, et al. Cancer-activated doxorubicin prodrug nanoparticles induce preferential immune response with minimal doxorubicin-related toxicity. *Biomaterials*. 2021;272:120791.